The Astrophysical Journal, 652:1563–1571, 2006 December 1

ACCRETION ONTO THE COMPANION OF η CARINAE DURING THE SPECTROSCOPIC EVENT. III. THE He II λ4686 LINE

Noam Soker and Ehud Behar
Department of Physics, Technion–Israel Institute of Technology, Haifa 32000, Israel; soker@physics.technion.ac.il, behar@physics.technion.ac.il
Received 2006 May 30; accepted 2006 August 9

ABSTRACT

We continue to explore the accretion model of the massive binary system η Car by studying the anomalously high He II λ4686 line. The line appears just before periastron and disappears immediately thereafter. Based on the He II λ4686 line emission from O stars and their modeling in the literature, we postulate that the He II λ4686 line comes from the acceleration zone of the secondary stellar wind. We attribute the large increase in the line intensity to a slight increase in the density of the secondary stellar wind in its acceleration zone. The increase in density could be due to the ionization and subsequent deceleration of the wind by the enhanced X-ray emission arising from the shocked secondary wind farther downstream or to accretion of the primary stellar wind. Accretion around the secondary equatorial plane gives rise to collimation of the secondary wind, which increases its density, hence enhancing the He II λ4686 emission line. In contrast with previous explanations, the model proposed in this paper does not require a prohibitively high X-ray flux to directly photoionize the He.

Subject headings: accretion, accretion disks — binaries: close — circumstellar matter — stars: individual (η Carinae) — stars: mass loss

1. INTRODUCTION

The massive stellar binary system η Carinae displays a periodicity of 5.54 yr in many emission lines and in the continuum, from the IR (e.g., Whitelock et al. 2004) to X-rays (Corcoran et al. 2001a, 2005, 2004; Corcoran 2005). The fading of high-excitation lines (e.g., Fe III λ1895, Fe III λ4701, Ne III $\lambda\lambda$1747–1754, and Si III λ1892 [Zanella et al. 1984]; He I λ10830 [Damineli 1996]; He I λ6678 [Damineli et al. 2000]; and many more lines listed by Damineli et al. [1998]) every 5.54 yr is assumed to occur near periastron passages, and it is termed the spectroscopic event (e.g., Damineli et al. 2000). The primary star of the η Car binary system is more massive and cooler than the hotter secondary companion, probably an O-type or a WR star (Iping et al. 2005). The primary wind is slower but has a higher mass-loss rate than the secondary wind. Although it is widely accepted that η Car is a binary system (e.g., Damineli 1996; Damineli et al. 1997, 2000; Ishibashi et al. 1999; Corcoran et al. 2001a, 2001b, 2005; Pittard & Corcoran 2002; Duncan & White 2003; Fernandez Lajus et al. 2003; Smith et al. 2004; Whitelock et al. 2004; Verner et al. 2005), the precise influence of the secondary on the outflowing gas, and in particular its role in shaping the bipolar nebula—the Homunculus—is only poorly understood. The $\gtrsim$10 $M_\odot$ Homunculus (Smith et al. 2003) was formed during the 1837–1856 Great Eruption and is now expanding outward at a velocity of $\sim$600 km s^{-1} (Davidson & Humphreys 1997). A weaker bipolar eruption occurred during the Lesser Eruption of 1890 (Ishibashi et al. 2003).

The similarity of the Homunculus morphology to the morphologies of many planetary nebulae and symbiotic nebulae suggests that during the Great Eruption the secondary accreted mass from the primary along the entire orbit and blew two jets, which shaped the Homunculus (Soker 2001, 2004). Unlike the case during the 19th-century Great Eruption, at present the companion does not accrete mass during most of its orbital motion. However, recently Soker (2005a, 2005b) has suggested that for several weeks near periastron passages the secondary does accrete mass from the primary. This accretion shuts down the secondary's wind and hence the X-ray emission, leading to the long X-ray minimum (Soker 2005a, 2005b; Akashi et al. 2006). The formation of an accretion disk in the present-day η Car binary system (albeit only for a short time; Soker 2003, 2005a) is in agreement with some of the suggestions made earlier by van Genderen et al. (1994, 1995, 1999).

According to the accretion model, the basic accretion process near periastron passages is as follows (Soker 2005b): The collision between the two winds creates (two) shock waves that heat the winds to X-ray temperatures, which later escape the system. The postshock primary wind material cools to a very low temperature, $\lesssim 10^4$ K, and is prone to instabilities that might lead to the formation of dense blobs. While during most of the 5.54 yr orbital period the secondary's gravity has a negligible effect on the winds, near periastron the collision region is close to the secondary star, and the secondary's gravitational field becomes significant, to the extent that the primary wind falls onto the secondary, which in turn accretes primary wind fragments. Namely, near periastron passage the collision region of the two winds is assumed to collapse onto the secondary star, a process that is further assumed to shut down the secondary wind (Soker 2005b). This substantially reduces the X-ray luminosity (Akashi et al. 2006). The accretion process may last somewhat longer than the $\sim$70 days of the X-ray deep minimum.

In the present paper, we wish to study the He II λ4686 emission line detected by Steiner & Damineli (2004, hereafter SD04) and by Martin et al. (2006, hereafter M06). In particular, we try to explain its sharp rise and subsequent decline around the η Car periastron. M06 attribute this to a temporary mass ejection or wind disturbance on the primary star. We instead attribute the emission to the wind of the secondary star and the variation in the He II λ4686 emission to variation in the properties of the secondary wind and to a collimated fast wind (CFW) blown by the secondary star. The onset of accretion accounts in our model for the disappearance of the He II λ4686 line during the X-ray minimum, when the secondary wind is shut down. In § 2, we examine the possible influence of the X-rays emitted by the shocked winds on

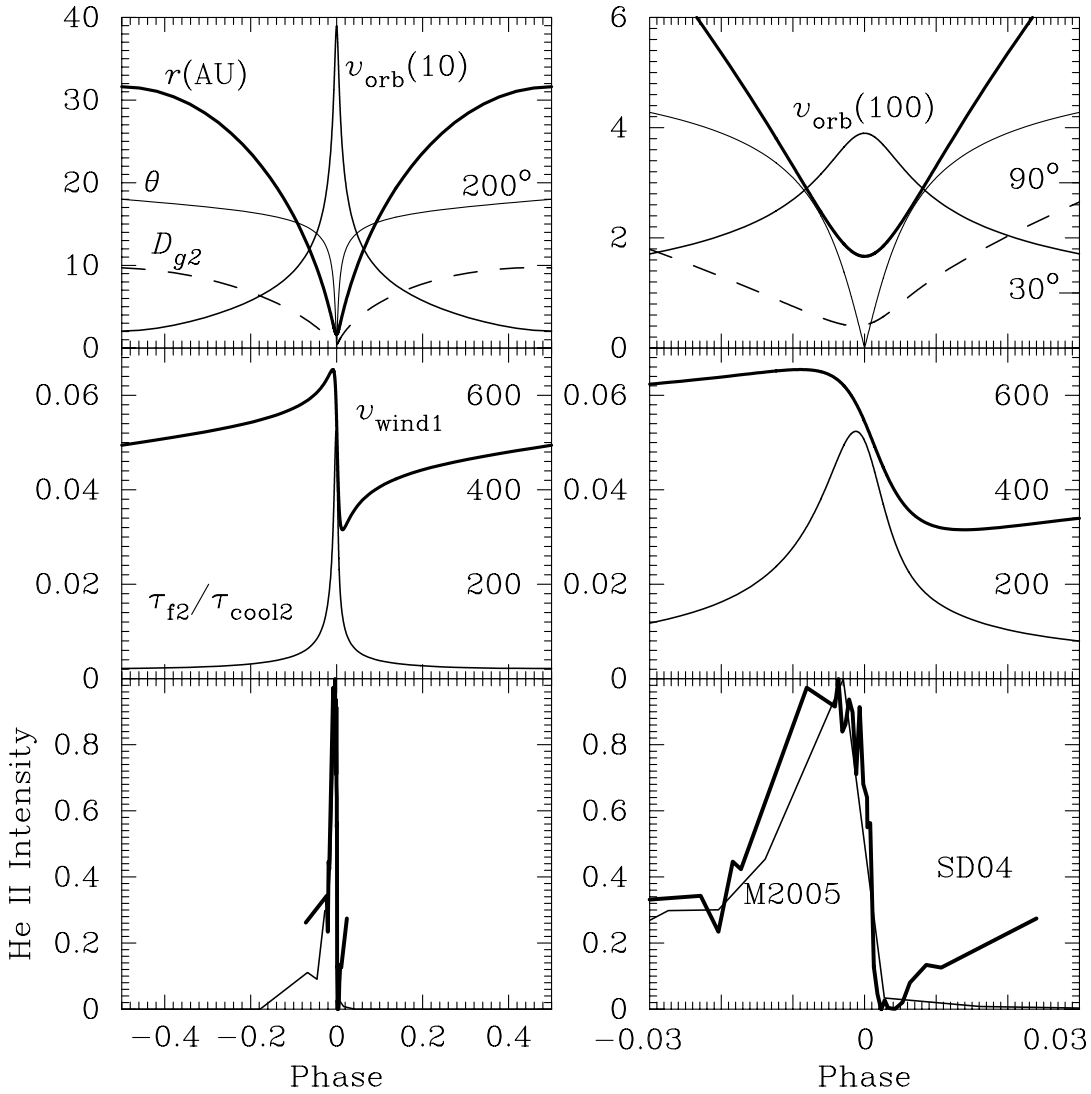

FIG. 1.—Several physical variables as a function of orbital phase. The left column covers the entire orbit, while the right column covers the time just prior to and after periastron. In the top two rows quantities are calculated from the model and phase zero is exactly at periastron. *Top row*: Orbital separation (*thick solid line*, in AU), distance of the stagnation point from the secondary D_{g2} (*dashed line*, in AU), orbital angle θ (*thin solid line*), and relative orbital speed of the two stars (*medium solid line*, in 10 km s^{-1} on the left and 100 km s^{-1} on the right). The angle θ is the relative direction of the two stars as measured from periastron (scale on the right in degrees). *Middle row*: *Thick line*, Velocity of the primary wind relative to the secondary $v_{\rm wind1}$ (scale on the right in km s^{-1}); *thin line*, ratio of the flow time of the shocked secondary wind out of the colliding wind region τ_{f2} to its radiative cooling time $\tau_{\rm col2}$. *Bottom row*: Intensity of the He II λ4686 line. The thick line depicts the equivalent width as given by SD04 for the time period when measurements are reliable, while the thin line is the He II λ4686 line intensity from M06. Both lines are scaled to their maximum value. In the bottom row phase zero is at 2003 June 29.

the secondary wind. The general properties of the He II λ4686 line and the outline of our proposed explanation are described in § 3. Our summary and predictions are presented in § 4.

2. X-RAY ILLUMINATION OF THE SECONDARY WIND

2.1. *The Binary System*

The η Car binary parameters are as in the previous two papers in this series (Soker 2005b; Akashi et al. 2006). The assumed stellar masses are $M_1 = 120\ M_\odot$ and $M_2 = 30\ M_\odot$, the eccentricity is $e = 0.9$, and orbital period is 2024 days; hence, the semimajor axis is $a = 16.64$ AU, and periastron occurs at $r = 1.66$ AU. The mass-loss rates are $\dot{M}_1 = 3 \times 10^{-4}\ M_\odot$ yr^{-1} and $\dot{M}_2 = 10^{-5}\ M_\odot$ yr^{-1}. The primary's wind profile is $v_1 = 500[1 - (0.4\ {\rm AU}/r_1)]$ km s^{-1}, where r_1 is the distance from the center of the primary. In the colliding wind region relevant to us, we can set $r_1 = r$, where r is the orbital separation between the two stars. The secondary's terminal wind speed is taken to be $v_2 = 3000$ km s^{-1}. The orbital separation r, the relative orbital velocity of the two stars $v_{\rm orb}$, the relative angle of the two stars measured from periastron, and the distance of the stagnation point of the colliding two winds from the secondary D_{g2} are plotted on the top row of Figure 1. In the middle row the velocity of the primary wind relative to the stagnation point $v_{\rm wind1}$ is depicted by the thick line. The thin line represents the ratio $\tau_{f2}/\tau_{\rm cool2}$, where τ_{f2} is the typical time for the shocked secondary wind to flow out of the shocked region (the winds' interaction zone), while $v_{\rm cool2}$ is the radiative cooling time of the shocked secondary wind. For more details on these quantities see Soker (2005b) and Akashi et al. (2006).

The secondary can be assumed to be an O star. Somewhat evolved main-sequence O stars with $M_2 = 30\ M_\odot$ can have an effective temperature of $T_{\rm eff} \simeq 40{,}000$ K and a luminosity of $L_2 \simeq 3 \times 10^5\ L_\odot$, and hence a radius of $R_2 \simeq 11\ R_\odot$; such stars have mass-loss rates of up to $\sim 10^{-5}\ M_\odot$ yr^{-1} (e.g., Repolust et al. 2004). These estimates are associated with large uncertainties,

since most likely the secondary underwent a massive accretion event $\sim$160 yr ago (Soker 2001), and hence it is likely to be out of thermal equilibrium. Recently, Verner et al. (2005) deduced the following secondary properties: $T_{\rm eff} \simeq 37,200$ K, $L_2 \simeq 9.3 \times 10^5\ L_\odot$, $R_2 \simeq 23.6\ R_\odot$, $v_2 = 2000$ km s^{-1}, and $\dot{M}_2 \simeq 8.5 \times 10^{-6}\ M_\odot$ yr^{-1}. We therefore scale the model with a value of $R_2 = 20\ R_\odot$.

In the first two papers in the series (Soker 2005b; Akashi et al. 2006), the acceleration zone of the secondary's wind was not considered, and it was assumed that the secondary wind encounters the shock wave at its terminal velocity. In fact, because of the nonnegligible acceleration zone, the secondary wind does not reach its terminal speed when it encounters the shock wave. This in turn reduces the distance between the stagnation point and the secondary, D_{g2}, and enhances the effect of accretion of the shocked primary wind near the stagnation point by the secondary. In the present paper, we treat the acceleration zone more carefully, as we believe it is in this region that the He II λ4686 line is formed, a possibility raised already by SD04. We adopt the following β velocity profile for the secondary's wind acceleration zone:

$$v_{2r}(r_2) = v_2 \left(1 - \frac{R_2}{r_2}\right)^{\beta}, \tag{1}$$

with $\beta = 1$, where r_2 is the distance from the center of the secondary, and $v_2 = 3000$ km s^{-1}. For the parameters assumed here, the gravitational acceleration on the surface of the secondary is $\log [g_2(\text{cm s}^{-2})] = 3.3$. In such stars, Venero et al. (2002) find more efficient acceleration and hence a narrower acceleration zone, which implies a lower column density through the wind with less X-ray absorption. The density profile is given by mass conservation, and for the parameters used here, $\dot{M}_2 = 10^{-5}\ M_\odot$ yr^{-1}, it is

$$\rho_2(r_2) = 9 \times 10^{-14} \left(\frac{r_2}{R_2}\right)^{-2} \left(\frac{R_2}{20\ R_\odot}\right)^{-2} \left(1 - \frac{R_2}{r_2}\right)^{-1} \text{g cm}^{-3}. \tag{2}$$

The column density from infinity inward to the secondary wind at radius r_2 is given by integrating over the proton number density $n_{p2} = \rho_2/m_p$,

$$N_{p2} = \int_{r_2}^{\infty} n_{p2}\, dr_2' = -5 \times 10^{22} \left(\frac{R_2}{20\ R_\odot}\right)^{-1} \ln\left(1 - \frac{R_2}{r_2}\right) \text{ cm}^{-2}. \tag{3}$$

As mentioned above, the acceleration of the secondary wind is likely to be larger than that given by equation (1); hence, the density will be lower than that given by equation (2), and the column density lower than that of equation (3).

The He II λ4686 line intensity very sensitively increases with increasing wind temperature T_0. In the different relevant models of Venero et al. (2002), the wind temperature $T_{\rm wind} = T_0$ spans the range 15,000–32,000 K. Consequently, we assume a fixed temperature of $T_0 = 20{,}000$ K. The velocity, density, and temperature profiles of the wind model are plotted in the top panel of Figure 2. The bottom panel shows the column density and optical depth into the wind.

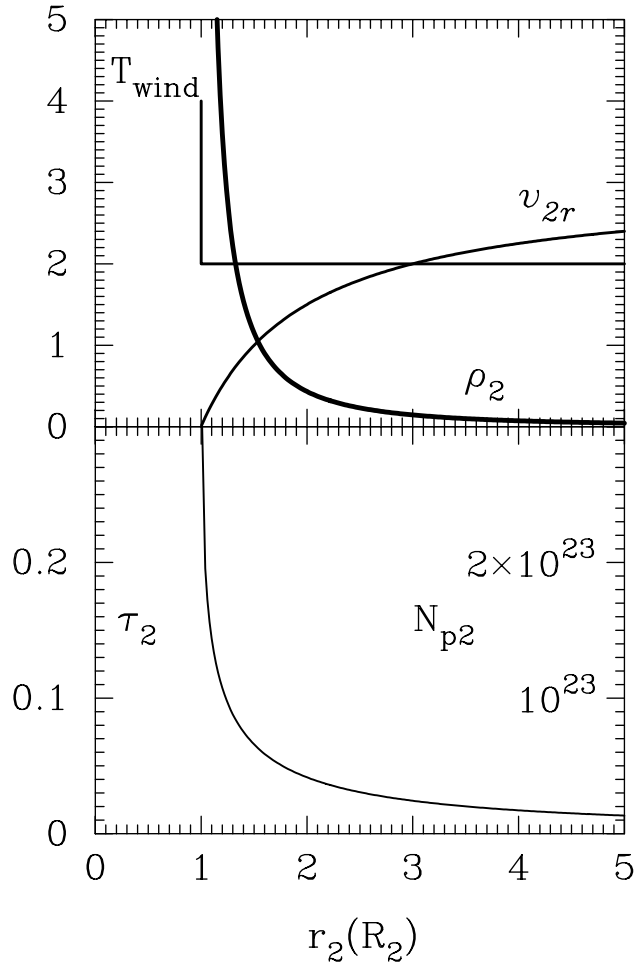

FIG. 2.—*Top*: Assumed secondary wind parameters. Shown are the wind velocity v_{2r} (in units of 1000 km s^{-1}), temperature $T_{\rm wind}$ (in units of 10,000 K), and density ρ_2 (in units of 10^{-13} g cm^{-1}) for a mass-loss rate of $\dot{M}_2 = 10^{-5}\ M_\odot$ yr^{-1}. The distance from the secondary center is in units of the secondary radius, taken to be $R_2 = 20\ R_\odot$. *Bottom*: Optical depth for radiation coming from infinity τ_2 (units on the left side) and proton column density N_{p2} (in units of cm^{-2} on the right side). Note that the same line represents both τ_2 and N_{p2}.

2.2. *X-Ray Emission*

The assumptions entering the calculation of the X-ray emission were summarized by Akashi et al. (2006), who were interested in the X-ray emission in the 2–10 keV band. Here too, we need to know the X-ray flux from both the primary and secondary shocked winds.

2.2.1. *Primary Wind*

We are interested in the X-ray emission close to minimum, i.e., periastron passage, where the shocked primary's wind is very dense and its cooling time is much shorter than the flow time (e.g., Pittard & Corcoran 2002; Soker 2003). Therefore, we can assume that the postshock primary's wind material near the stagnation point cools instantaneously by emitting all its thermal energy. During the pre–X-ray minimum the primary wind speed relative to the stagnation point is $v_{\rm wind1} \simeq 600$ km s^{-1}, corresponding to a postshock temperature of $T_{s1} \simeq 5 \times 10^6$ K, while after the X-ray minimum the preshock primary wind speed is $v_{\rm wind1} \simeq 400$ km s^{-1}, corresponding to postshock temperatures of $T_{s1} \simeq 2.2 \times 10^6$ K (this is evident in Fig. 3, *dashed line*, to be discussed below).

From the shape of the shock front of the primary wind, Akashi et al. (2006) estimate the fraction of the primary wind that is strongly shocked and that contributes most to the X-ray emission

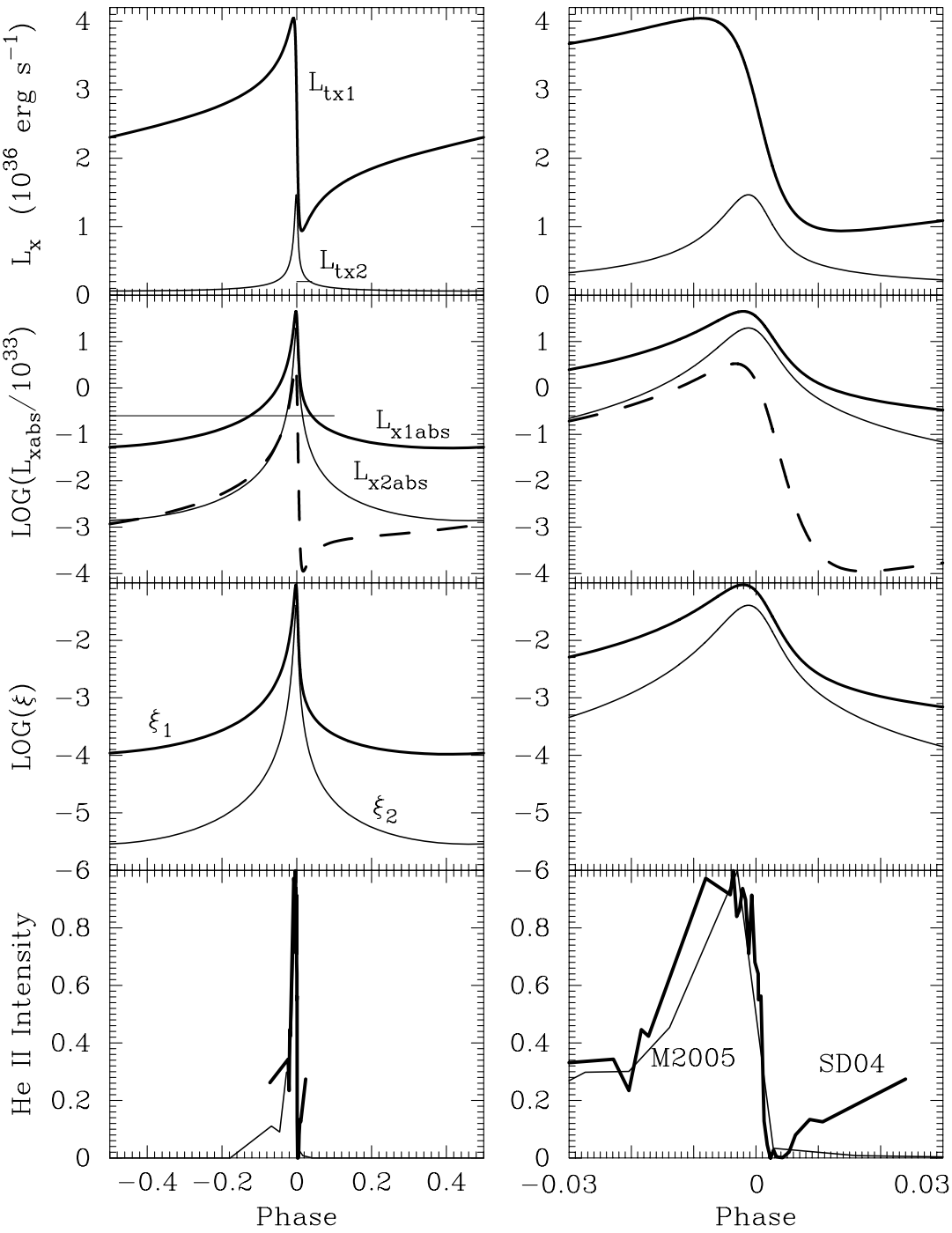

FIG. 3.—*Top row*: Total X-ray luminosity of the postshock winds, the primary wind $L_{t,\rm X1}$ (*thick line*) and the secondary wind $L_{t,\rm X2}$ (*thin line*), both in units of 10^{36} ergs s^{-1}. The time that the secondary wind does not exist in the accretion model for the minimum is marked by a short horizontal line in the left panel (in the orbital-phase range 0–0.04). *Second row*: Fraction of the total X-ray emission that would be absorbed by the secondary star, for $R_2 = 20\ R_\odot$, if no absorption in the secondary wind occurs. The dashed line shows the contribution of the X-rays emitted by the primary postshock wind above 1 keV. All three lines are in units of 10^{33} ergs s^{-1} and in logarithmic scale. The long horizontal line is drawn to emphasize the stronger X-ray emission before periastron compared with after periastron. *Third row*: Ionization parameter defined in eq. (6) calculated close to the secondary photosphere at $r_2 = 1.05R_2$, where the nucleon number density is $n_n \simeq 10^{12}$ cm^{-3}, and for $r_{\rm X} = D_{g2}$, in logarithmic scale and units of ergs cm s^{-1}. *Bottom row*: He II λ4686 line intensity as in the bottom row of Fig. 1.

to be $k_1 \simeq 0.1$. The total X-ray emission of the shocked primary wind is therefore

$$L_{t,\rm X1} \simeq 3.4\times10^{36}\left(\frac{k_1}{0.1}\right)\left(\frac{\dot M_1}{3\times10^{-4}\ M_\odot\ \rm yr^{-1}}\right) \times\left(\frac{v_{\rm wind1}}{600\ \rm km\ s^{-1}}\right)^2 \rm ergs\ s^{-1}. \quad (4)$$

The value of $L_{t,\rm X1}$ as a function of orbital phase is shown as a thick line in the top row of Figure 3.

Assuming that the emission is concentrated near the stagnation point and neglecting absorption by the material near the stagnation point, we derive the radiation power that is absorbed by the secondary $L_{\rm X1,abs} = 0.5L_{t,\rm X1}(R_2/D_{g2})^2$. The variation of $L_{\rm X1,abs}$ with orbital phase for $R_2 = 20\ R_\odot$ is shown by the thick line in the second row of Figure 3. The dashed line in that plot shows the

contribution of X-rays above 1 keV to $L_{\rm X1,abs}$. In order to make the asymmetry around periastron passage clear, we draw a horizontal line at the absorbed power value of 2.5×10^{32} ergs s^{-1}. This shows that the X-ray emission is stronger before the spectroscopic event than after it.

2.2.2. *Secondary Wind*

The radiative cooling time of the postshock secondary wind material $\tau_{\rm cool2}$ is much longer than its flow time out of the wind-collision region. Like Akashi et al. (2006), we assume that about half of the mass blown by the secondary star is shocked in a perpendicular shock front and that the total emitted energy is a fraction $k_2\tau_{f2}/\tau_{\rm cool2}$ of the thermal energy of the postshock gas. Here $\tau_{f2}\equiv D_{g2}/v_2$ is the characteristic flow time of the shocked wind out of the interaction region (Soker 2005b). The value of $\tau_{f2}/\tau_{\rm cool2}$ is plotted in the middle row of Figure 1. By fitting the X-ray luminosity to observations, Akashi et al. (2006) obtain $k_2=2$. The contribution of the shocked secondary wind material to the X-ray luminosity is therefore

$$L_{t,\rm X2}=1.4\times10^{35}\left(\frac{\dot{M}_2}{10^{-5}\ M_\odot\ {\rm yr}^{-1}}\right)\left(\frac{v_2}{3000\ {\rm km\ s}^{-1}}\right)^2\times\left(\frac{k_2\tau_{f2}/\tau_{\rm cool2}}{0.01}\right)\ {\rm ergs\ s}^{-1}. \quad (5)$$

This is much smaller than $L_{t,\rm X1}$. However, the secondary wind velocity and thus the postshock temperatures are much higher, corresponding to $T_{s2}=1.3\times10^8$ K. Consequently, the X-ray radiation produced by the secondary wind is much harder and its transmission through the primary wind much higher. The value of $L_{t,\rm X2}$ as a function of orbital phase with $k_2=2$ is shown by the thin line in the top row of Figure 3.

Assuming that the emission is concentrated in the region approximately D_{g2} away from the secondary and neglecting absorption by the shocked secondary wind, we derive the radiation power of the secondary wind that is absorbed by the secondary star $L_{\rm X2,abs}=0.5L_{t,\rm X2}(R_2/D_{g2})^2$. The variation of $L_{\rm X2,abs}$ with orbital phase for $R_2=20\ R_\odot$ is shown by the thin line in the second row of Figure 3. SD04 already noted that the sharp rise in the X-rays and its absorption by the secondary star might be the reason for the rapid rise in the He II λ4686 line intensity.

2.3. *Influence of X-Rays on Secondary Wind*

2.3.1. *Wind Velocity*

The influence of X-rays incident upon an O-star wind was studied by Stevens & Kallman (1990, hereafter SK90) in the context of high-mass X-ray binaries. For the typical physical values appropriate for η Car, the results of SK90 imply that the X-rays do not penetrate the wind deep enough to influence the mass-loss rate. However, the X-rays do ionize the wind and thus reduce the efficiency of the radiative acceleration of the wind. Hence, in the presence of X-rays, the wind in the acceleration zone is slower and denser. The important parameter that determines the wind ionization by X-rays is the photoionization parameter, which is defined as (SK90)

$$\xi=\frac{L_{\rm X}}{n_n r_{\rm X}^2}=4.5\times10^{-3}\left(\frac{L_{\rm X}}{10^{36}\ {\rm ergs\ s}^{-1}}\right)\left(\frac{n_n}{10^{12}\ {\rm cm}^{-3}}\right)^{-1}\times\left(\frac{r_{\rm X}}{1\ {\rm AU}}\right)^{-2}\ {\rm ergs\ cm\ s}^{-1}, \quad (6)$$

where $r_{\rm X}$ is the distance from the X-ray source and n_n the nucleon number density. We are interested in the effect of photoionization by the primary and secondary shocked winds on gas just off the surface of the secondary, where its wind is launched. Thus, we take $r_{\rm X}=D_{g2}$ and $n_n=10^{12}$ cm^{-3} (appropriate for $r_2=1.05R_2$; see eq. [2]). The resulting ionization parameter as a function of orbital phase is drawn in the third row of Figure 3 for photoionization due to both the primary (ξ_1, *thick line*) and secondary (ξ_2, *thin line*) shocked winds.

Learning from the results of SK90 (their Fig. 8 and Table 2), who use a temperature of 10 keV for the X-ray emitting gas, which is similar to that of the shocked secondary wind, we find that for $r_2\sim1.5R_2$, a typical region where the He II λ4686 emission forms, the X-rays start slowing down the secondary wind when $\xi\simeq10^{-4}$ ergs s^{-1} cm. For $\xi=10^{-3}$ ergs s^{-1} cm, the wind speed is $\sim$10% lower than its undisturbed velocity, while for $\xi=3\times10^{-3}$ ergs s^{-1} cm, it is $\sim$25% slower. All the values of ξ cited above are calculated at $r_2=1.05R_2$ (the relevant emitting region is at $r_2\sim1.5R_2$), as required for comparing with the results of SK90. The mass-loss rate does not change. Therefore, without considering other effects, the third row in Figure 3 suggests that the secondary wind will slow down and become denser approximately between phase -0.05 and $+0.04$. We postulate that at this time, the He II λ4686 line intensity will be enhanced.

When X-ray absorption by the secondary wind is taken into account, the effect of the soft X-rays from the shocked primary wind (i.e., ξ_1) is eliminated. The proton column density from infinity to the relevant region $r_2\simeq1.5R_2$ is $N_{p2}\sim5\times10^{22}$ cm^{-2}. For this column density, practically all X-ray emission below $\sim$1 keV (e.g., primary shocked wind) will thus be absorbed before reaching this region. Only the much harder X-rays emanating from the shocked *secondary* wind can reach $r_2\simeq1.5R_2$ and affect the secondary wind by means of ξ_2. SK90 consider both absorption and harder X-ray radiation. To estimate the influence of absorption on the secondary wind X-rays we compare Figure 6 of SK90 with their Figure 1, and for harder X-ray emission their Figure 7 with their Figure 1. Crudely, a column density of $N_{p2}\sim5\times10^{22}$ cm^{-2} reduces ξ_2 by a factor of $\sim$20. Our assumptions, on the other hand, underestimate ξ: (1) The optical depth should actually be calculated from $r_2=D_{g2}$ inward, making its real value smaller and the influence of the X-ray emission higher. However, for our goal it is adequate to use the column density from infinity and to avoid unnecessary complications, remembering that we overestimate X-ray absorption by the secondary wind. (2) We also underestimate the influence of the X-ray emission by taking the X-ray source to be at the stagnation point, at a distance D_{g2} from the center of the secondary. The secondary wind shock wave is actually closer to the secondary than the contact discontinuity surface, by a factor of $\sim$2 (Akashi et al. 2006). Overall, we estimate that the third row of Figure 3 overestimates ξ_2 by a factor of $\sim$3–10 (ξ_1 is negligible after absorption). Considering the many uncertainties involved, we cautiously propose that as periastron passage approaches, say after orbital phase ~-0.05, i.e., 100 days within periastron passage, the X-ray emission from the shocked wind can slow down the secondary wind by up to a few tens of percent.

2.3.2. *Wind Temperature*

Venero et al. (2002) find that the He II λ4686 emission line intensity is sensitive to the wind temperature and increases as the wind temperature increases and/or as the region of maximum temperature in the wind moves outward. We therefore examine the heating of the wind by X-rays. We neglect heating by the optical + UV energy flux of the primary star because the primary

optical + UV spectrum is similar to that of the secondary star, but its flux is much smaller than the secondary flux in the relevant region at $r_2 \sim 1.5R_2$. The X-ray emission, on the other hand, is much harder and ionizes and heats the gas.

As can be seen in Figure 15 of Venero et al. (2002) an increase of $\sim$1000 K of the wind temperature can substantially increase the He II λ4686 emission line intensity. Say a fraction δ of the X-rays absorbed by the secondary wind go to heat. The particle number loss rate by the wind in the hemisphere facing the X-ray source is $\dot{M}_2/(2\mu m_{\rm H})$, where $\mu m_{\rm H}$ is the mean mass per particle. Therefore, the X-rays raise the wind temperature by

$$\Delta T_w \sim \delta \frac{2}{3k_{\rm B}} \frac{L_{\rm X,abs}}{\dot{M}_2/(2\mu m_{\rm H})} = 1500 \frac{\delta}{0.1} \left(\frac{L_{\rm X,abs}}{10^{33}\ {\rm ergs\ s^{-1}}} \right) \left(\frac{\dot{M}_2}{10^{-5}\ M_\odot\ {\rm yr^{-1}}} \right)^{-1} {\rm K}, \quad (7)$$

where $k_{\rm B}$ is the Boltzmann constant. Near the He II λ4686 maximum $L_{\rm X,abs} \sim 10^{33}$ ergs s^{-1}, and even for 5% efficiency, $\delta \sim 0.05$, the heating of the wind might be important. However, it seems that raising the wind temperature cannot be the main effect causing the variation in the He II λ4686 line intensity.

3. THE PROPOSED MODEL FOR THE He II λ4687 LINE

3.1. *The* He II *λ4686 Line in η Car*

The general binary model for our purposes is described in the first two papers of the series (Soker 2005b; Akashi et al. 2006). The dependence of some relevant binary parameters on the orbital phase, with phase zero at periastron, is drawn in the top and middle rows of Figure 1. The bottom row of Figure 1 shows the behavior of the He II λ4687 emission line. The thin line depicts the He II line intensity as given by M06, while the thick line is the equivalent width from SD04, giving only the time period when measurements are reliable (A. Damineli 2005, private communication). Both lines are normalized to their maximum intensity. Following the discussion by M06 of the problematic continuum assessment of SD04, we refer more to the He II λ4686 intensity as given by M06, in which there is no rise in intensity after the peak. Note that in our modeling, phase zero is well defined at periastron. This is not to be confused with phase zero defined from observations of the intensities of different lines (2003 June 29, JD = 2,452,819.8); in the latter case phase zero is assumed to be near periastron, but it is not well defined (see footnote 6 in M06).

Three qualitative regimes are seen in the intensity evolution.

1. *No emission*.—During most of the orbit the He II intensity is very weak, practically zero, although we note that M06 discuss the slight possibility that Thackeray (1953) detected the line in weak emission.

2. *Slow rise*.—At orbital phase ~ -0.1 ($\sim$200 days before periastron passage) the intensity starts to rise slowly. M06's first detection is $\sim$140 days before the spectroscopic event. (In Fig. 1, *bottom*, we connected the observation points of M06 and the previous measurement to the first detection 220 days earlier.) The staring point of the slow rise is the main discrepancy between SD04 (slow rise started almost a year before minimum) and M06 (slow rise started $\sim$5 months before minimum).

3. *Peak*.—At orbital phase ~ -0.02 ($\sim$40 days before periastron passage) the intensity sharply rises to its maximum value at phase ~ -0.006 after which it sharply declines back to its minimum value (SD04). With inferior temporal resolution, M06 quote a phase of -0.004 for the peak. The He II peak is not as well located as the narrow X-ray flares, but it seems to occur when the X-ray intensity is dropping (M06). Namely, as the X-ray source is shut down, the He II λ4686 line gains its intensity. Then both X-ray and He II λ4686 intensity are at their minimum.

After correcting for extinction by a factor of about 100, SD04 find the peak luminosity of the He II λ4686 line to be $L_{\rm He\,II} \sim 100\ L_\odot$, which amounts to $\dot{N}_{\rm He\,II} \sim 9 \times 10^{46}$ photons s^{-1} in the line alone. M06 find the peak luminosity to be $\sim$2.5 times higher at 1.4×10^{36} ergs s^{-1}. Since M06 did not observe η Car at the exact maximum, the true He II λ4686 maximum could be even higher than this. Noting that the X-rays and He II λ4686 line rise together before the X-ray luminosity drops, SD04 suggest that the X-rays can account directly for the He II emission by ionizing the helium. SD04 extrapolate the X-ray spectrum in the energy range 1 keV $< E_\gamma <$ 10 keV as given by Corcoran and collaborators (Ishibashi et al. 1999; Corcoran et al. 2001b; Pittard & Corcoran 2002) down to $E_1 = 54$ eV, the ionization threshold of He^+. We used the APEC plasma compilation (Smith et al. 2001) to calculate the photon flux from 54 eV to 10 keV for plasma at the temperature of $\sim 5 \times 10^6$ K appropriate for the shocked primary wind (the secondary wind supplies a much smaller number of photons). We get 1.7×10^9 photons erg^{-1} in this range (as would be expected $\sim$1 photon keV^{-1}). At maximum, the X-ray luminosity of the shocked primary wind is $L_{t,\rm X1} \simeq 4 \times 10^{36}$ ergs s^{-1}, which implies an ionizing photon number rate of $\sim 7 \times 10^{45}$ s^{-1}. Before even considering the solid angle occupied by the secondary wind and the efficiency of He II λ4686 line formation, there is an order-of-magnitude deficiency in photons. When considering the efficiency of line formation the number of ionizing photons from the X-ray emitting gas is found to be more than 2 orders of magnitude below the required ionization flux to explain the He II λ4686 line. Therefore, as already noted by M06, another explanation is required for the He II λ4686 emission.

Another problem with the X-rays directly ionizing the He is that the observed He II λ4686 line maximum occurs 18 days after the observed X-ray flux starts to decline to its deep minimum. This point was raised by M06, and we reinforce it here by arguing that this decline in X-ray flux must be intrinsic to the X-ray source. Indeed, in Akashi et al. (2006), in which we modeled the X-ray light curve of η Car, we found that the decrease in X-ray luminosity at phase -0.015 ($\sim$30 days before periastron) has to be intrinsic to the X-ray source and cannot be explained by absorption toward our line of sight. The results of Akashi et al. (2006) thus rule out the possibility that the He gas sees a strong steady X-ray source while we observe the deep X-ray minimum. In summary, X-ray ionization of the He gas appears to be highly unlikely.

Both SD04 and M06 find that the He II λ4686 line is blueshifted. SD04 have better time sampling and find the line-of-sight velocity to rise from $\sim$100 to $\sim$400 km s^{-1} at its maximum intensity. Stahl et al. (2005) observed the reflection of emission from the polar direction and consider the He II λ4686 line to be formed in a shock front. They too find the He II λ4686 line to be blueshifted. This behavior of the He II λ4686 line and its rapidly evolving blueshift show that this velocity cannot be attributed to the orbital motion of the secondary star but must originate from genuinely outflowing gas, perhaps in a biconical flow. The redshifted part of the flow then must be obscured. In our model, the He II λ4686 line is formed close to the secondary star. Therefore, the star itself will block any redshifted emission, if it exists.

M06 discuss three possibilities for the He II line emission: in the colliding wind region, in a dense shell ejected by the primary star during the early spectroscopic event, or a combination of

the two. In any case, it seems that an enhanced mass-loss rate by the primary is required in their suggestion. M06 require the enhanced mass-loss rate from the primary to temporarily be several $\times 10^{-3}\,M_{\odot}\,\mathrm{yr}^{-1}$ for a wind speed of $v_1 = 700$ km s^{-1}. They note that in their suggested scenario for the He II λ4686 line the energy supply appears to be marginal and requires radiative processes to enhance the He II λ4686 line formation. In summary, we find neither the explanation by SD04 nor those by M06 for the He II λ4686 emission to be realistically satisfactory.

3.2. *The Proposed Model*

Many O stars are known to have strong emission in the He II λ4686 line, with an equivalent width of 1–3 Å (e.g., Grady et al. 1983), which translates into a line luminosity of $\sim 10\,L_{\odot}$. The stars in the sample of Grady et al. (1983) have mass-loss rates lower by at least a factor of 5 than does the secondary in the η Car system, and their bolometric luminosity is $\simeq L_2$ as given be Verner et al. (2005). The He II λ4686 line in the sample of Grady et al. (1983) displays velocities in the range of 0–600 km s^{-1}. Similar blueshifted velocities were inferred by SD04 for η Car. Grady et al. (1983) argue that the He II λ4686 line intensity variability is connected to changes in the entire wind acceleration zone. The changes in the acceleration zone can be in the ionization balance and the mass-loss rate (e.g., Venero et al. 2002). Kunasz (1980) found that when the He II λ4686 line is only slightly in emission it is very sensitive to the wind parameters. This is most likely the case in η Car, where the He II λ4686 does not exist most of the time and appears only several months before the spectroscopic event (M06). Late WNL stars, whose hydrogen abundance is lower by a factor of a few relative to solar, are also known to be strong He II λ4686 emitters, with line luminosity of up to several $\times 100\,L_{\odot}$ (Crowther 2000). This sensitivity of the He II λ4686 to wind parameters under particular conditions implies that the variations in this line might come with unnoticeable variations in other lines. Furthermore, time variability in some lines in WR stars is known to be unrelated to variability in the He II λ4686 line, e.g., N V λ4945 and C IV λ5806 (Morel et al. 1999). In a sample of seven O stars Ninkov et al. (1987) find the variation in the equivalent width of the C III λ5696 line from star to star to be unrelated to the variation in the equivalent width of the He II λ4686 line. The variation of the N III $\lambda\lambda$4634–4641 (multiplet) is also weakly related to the He II λ4686 line. Different lines are formed at different locations in the wind and therefore are influenced differently as the system approaches periastron. Indeed, Rauw et al. (2001) studied the O7.5 I + ON9.7 I binary system HD 149404 and found the He II λ4686, C III λ5696, N III $\lambda\lambda$4634–4641, N III $\lambda\lambda$5932, 5942, and S IV $\lambda\lambda$4486, 4504 lines to originate from different locations in the binary system. Rauw et al. (2005) find temporal and spacial correlations between the He II λ4686 line and Hα in the very massive binary system WR 20a (WN6ha + WN6ha). We therefore do not necessarily expect variability in the intensity of all other lines to follow that of the He II λ4686 line, although it is possible that some lines show qualitatively similar behavior.

Having compared the properties of these O stars from the literature with those of η Car, we suggest that the He II λ4686 line is formed in the acceleration zone of the secondary wind. That the He II λ4686 line originates in the acceleration zone of the secondary wind has been proposed by SD04. However, there is a fundamental difference between our model and theirs. In our model, the energy source for the He line is the outflowing secondary wind and not the X-ray emission as suggested by SD04. The energy in the He II line is negligible compared to the kinetic energy of the wind, and as with the O stars mentioned above, the energy in the He II λ4686 line results from excitation and ionization processes within the accelerated wind. Therefore, there is no energy budget crisis in our model. The assumption that the He II line results in the acceleration zone of the secondary wind accounts for the behavior of the He II λ4686 emission line as follows.

1. *No emission*.—During most of the orbit the conditions in the secondary wind are such that the line is very weak. (Theoretical calculations by Kunasz [1980] show that the line might even appear in absorption.) However, the conditions are such that a slight increase in the density and/or temperature in the acceleration zone will lead He II λ4686 to show up in emission.

2. *Slow rise*.—As the two stars approach each other the ionization parameter (ξ_2) due to the secondary X-rays increases such that enough X-rays penetrate to the acceleration zone, i.e., the ionization parameter in the acceleration zone of the secondary wind exceeds 10^{-4} ergs s^{-1} cm. Consequently, the wind speed decreases while the mass-loss rate is unaffected, as discussed in § 2.3.1. This results in a higher density in the acceleration zone, which based on the results of Kunasz (1980) increases the intensity of the He II λ4686 emission line. In addition, the X-rays raise the wind temperature by several hundred kelvins (§ 2.3.2). This slightly higher wind temperature also increases the He II λ4686 line intensity (Venero et al. 2002). We note that it is sufficient for the mass-loss rate (Kunasz 1980) or the temperature in the wind's acceleration zone (Venero et al. 2002) to increase slightly in order to substantially strengthen the He II line. The full modeling of these processes requires a stellar structure code and is much beyond the scope of the present paper, but the results of § 2 do suggest that the X-ray emission from the colliding wind can influence the wind speed and temperature, which in turn can drastically change the He II λ4686 line intensity.

Another effect, not treated in § 2, is the possibility that dense blobs are accreted from the postshock primary wind region (Soker 2005b). As these blobs fall into the secondary wind acceleration region, they will form shock waves in the secondary wind. This will further heat the wind and in a limited region would further enhance the He II line.

3. *Peak*.—According to our model, for $\sim$70 days, the secondary accretes from the primary wind (Soker 2005b) after the collapse of the shocked primary wind material in the region of the stagnation point onto the secondary. As we show below, this gas has high specific angular momentum. The collapse starts at phase ~ -0.02, namely, $\sim$40 days before periastron passage (Akashi et al. 2006); the X-ray minimum starts at phase $\sim$0. Since most of the gas is first accreted near the equatorial plane around the secondary, for a limited time it collimates the secondary wind toward the polar directions. The higher density in this collimated wind further enhances the intensity of the He II λ4686 line by a large factor (Kunasz 1980), leading to the peak in the He II λ4686 line intensity. This collimated wind could also be the low-energy analog of the X-ray jet (Behar et al. 2006). After the short peak, the secondary wind is totally shut down (Soker 2005b; Akashi et al. 2006), and hence the He II λ4686 line and the X-rays are shut down as well. After periastron when the secondary wind is resurrected (and the X-rays return) the secondary wind is back to its initial pre-accretion form, in which the He II line does not exist. In this phase we expect to see only the blueshifted (approaching) side of the collimated wind. The reason is that the inclination of η Car is $i = 42^{\circ}$ (i.e., the orbital plane is tilted by 48° from an edge-on view; Smith 2002), and the

He II λ4686 line is formed very close to the stellar surface, $r_2 \sim 1.5R_2$. Therefore, the star itself will block most of the He II λ4686 redshifted line, and the rest will be blocked by the dense region at the base of the wind at $R_2 < r_2 \lesssim 1.2R_2$.

The sharp decrease of the He II λ4686 line by a factor of $\sim$5–10 over about 10 days is accounted for by (1) the quick dying out of the secondary wind and (2) the speed of the secondary wind entering the shock being much lower. The lower speed is due to the X-ray ionization and heating, as well as to the stagnation region moving closer to the acceleration zone. The X-ray radiation will therefore be softer and hence more absorbed, and hence it will have a lesser affect on the acceleration zone.

We note that M06 briefly mention that the line might be formed by the winds of the two stars; they mainly consider the primary wind. However, M06 assume that the He II emission originates from photoionized regions near the X-ray shock fronts. The problem with this assumption, as noted by M06, is that the He II λ4686 line peak occurs well after the X-ray emission has started to drop. SD04 also considered this possibility, but they also considered an alternative in which the He II λ4686 originates in the acceleration zone of the secondary wind. We agree with this second suggestion of SD04.

We end this subsection by emphasizing again three points of our model. (1) The He II λ4686 is formed in the acceleration zone of the secondary wind. The sensitivity of this line to wind properties (Kunasz 1980; Venero et al. 2002) implies that changes in only a fraction of the acceleration zone can lead to a large variation in the line intensity. (2) The primary star has no direct role in the changes in the He II line properties; its only role is in supplying the gas that collides with the secondary wind, leading to X-ray emission, and in supplying the accreted gas during the accretion phase. (3) The energy in the He II line comes from the wind and the secondary star. Both the kinetic power in the secondary wind and the secondary luminosity are much larger than the maximum He II line luminosity. Therefore, there is no problem in supplying the energy to this line.

3.3. *Specific Angular Momentum*

We show now that the gas in the stagnation point has indeed enough specific angular momentum to be accreted from the equatorial plane, which could form a collimated wind or even two opposite jets. We take the shocked primary wind near the stagnation point to move slowly relative to the stagnation point; hence, it is corotating with the binary orbit at an angular velocity $\omega_b = v_{\rm peri} r_{\rm peri}/r^2$, where $v_{\rm peri}$ is the binary relative velocity at periastron and $r_{\rm peri}$ is the orbital separation at periastron. The specific angular momentum of the matter near the stagnation point around the secondary is $j_{s1} = D_{g2}^2 \omega_b$. For the relevant orbital phases we see from Figure 1 that $r/D_{g2} \simeq 4$, from which we find $j_{s1} \simeq 0.06 v_{\rm peri} r_{\rm peri}$. To check the degree to which the accretion onto the secondary departs from sphericity and whether an accretion disk might form, j_{s1} should be compared with the specific angular momentum of a test particle performing Keplerian motion on the secondary equator $j_2 = (G M_2 R_2)^{1/2}$. Substituting $v_{\rm peri} \simeq 390$ km s^{-1}, $r_{\rm peri} = 1.66$ AU (Fig. 1), and $M_2 = 30\ M_\odot$ we find

$$\frac{j_{s1}}{j_2} \simeq 0.8 \left(\frac{R_2}{20\ R_\odot} \right)^{-1/2}. \quad (8)$$

This shows that the collapsing material at the beginning of the accretion phase (and only at the beginning, before the Bondi-Hoyle type accretion takes place) has large enough specific angular momentum that most of the gas is accreted from near the equator. This will force the secondary wind to flow along the poles and hence have a much higher density at the wind base. Such a high density might substantially increase the He II λ4686 line luminosity (Kunasz 1980). Shortly after the collapse stage, the secondary wind is shut down, reducing to zero the He II λ4686 line and the X-ray emission. Formation of an accretion disk is marginal, and more accurate calculations are required to check whether an accretion disk can be formed and whether two opposite jets might be launched. This ends our explanation of the He II λ4686 emission peak.

4. DISCUSSION AND SUMMARY

In the present paper we continue to explore the different aspects of the winds' interaction in the massive binary system η Car and study the anomalously high He II λ4686 line appearing just before periastron and quickly disappearing immediately thereafter. Based on the He II λ4686 line emission from O stars and their modeling in the literature, we postulate that the He II λ4686 line comes from the acceleration zone of the secondary stellar wind. The large increase in the He II λ4686 line intensity is attributed to small changes in the properties of the secondary stellar wind. We suggest that the formation and acceleration of the secondary stellar wind is affected by the winds' interaction in two ways.

The first effect is due to the enhanced X-rays emitted by the shocked secondary wind. The secondary stellar wind is shocked as it encounters the primary stellar wind. The X-ray emission could reduce the acceleration of the secondary stellar wind (§ 2.3.1; see also SK90) and hence increase its density in the acceleration zone, which also heats the wind. Under the appropriate conditions, which we suggest exist in the acceleration zone of the secondary wind in η Car, higher density (Kunasz 1980) and/or higher temperature (Venero et al. 2002) increase the intensity of the He II λ4686 line emission.

The second effect is due to the accreted primary stellar wind, which affects the geometry of the secondary wind. Close to periastron passage, the secondary star starts to accrete from the shocked primary stellar wind (Soker 2005b; Akashi et al. 2006). Because of the high specific angular momentum of this accreted gas (eq. [8]), it will be accreted from near the equatorial plane. The equatorial accreted mass will collimate the secondary wind along the polar directions and might even form an accretion disk and launch two opposite transient jets, as suggested recently by X-ray observations (Behar et al. 2006). The polar outflow from the secondary will have much higher densities than the isotropic wind, and it is therefore expected to be a much stronger He II λ4686 emitter.

Our explanation for the temporal evolution of the He II λ4686 line is given in § 3.2. The explanation proposed in this paper for the He II λ4686 high intensity disputes previous ones (SD04; M06), which entailed photoionization of He exclusively by the X-rays. We agree, on the other hand, with the other suggestion of SD04 that the He II λ4686 line originates in the acceleration zone of the secondary wind and that the slow rise to maximum occurs on the side facing the winds' interaction zone. The high observed intensity of over 10^{53} line photons emitted over a period of about 20 days—while the X-ray flux is sharply dropping—implies a prohibitively high photoionizing X-ray flux, which the present model does not require.

Finally, we note that the influence of the X-ray emission on the secondary stellar wind, in making its velocity lower, will cause the stagnation point to be closer to the secondary star than was

assumed in earlier papers in the series (Soker 2005b; Akashi et al. 2006). Although this effect is not large, it reinforces accretion of primary shocked wind material near periastron, the key element in the accretion model.

We thank an anonymous referee for useful comments. This research was supported by a grant (28/03) from the Israel Science Foundation and by a grant from the Asher Space Research Institute at the Technion.

REFERENCES

Akashi, M., Soker, N., & Behar, E. 2006, ApJ, 644, 451
Behar, E., Nordon, R., Ben-Bassat, E., & Soker, N. 2006, preprint (astro-ph/0606251)
Corcoran, M. F. 2005, AJ, 129, 2018
Corcoran, M. F., Ishibashi, K., Swank, J. H., & Petre, R. 2001a, ApJ, 547, 1034
Corcoran, M. F., Pittard, J. M., Stevens, I. R., Henley, D. B., & Pollock, A. M. T. 2005, in X-Ray and Radio Connections, ed. L. O. Sjouwerman & K. K. Dyer (Charlottesville: NRAO), http://www.aoc.nrao.edu/events/xraydio/meetingcont/2.2_corcoran.pdf
Corcoran, M. F., et al. 2001b, ApJ, 562, 1031
———. 2004, ApJ, 613, 381
Crowther, P. A. 2000, A&A, 356, 191
Damineli, A. 1996, ApJ, 460, L49
Damineli, A., Conti, P. S., & Lopes, D. F. 1997, NewA, 2, 107
Damineli, A., Kaufer, A., Wolf, B., Stahl, O., Lopes, D. F., & de Araujo, F. X. 2000, ApJ, 528, L101
Damineli, A., Stahl, O., Kaufer, A., Wolf, B., Quast, G., & Lopes, D. F. 1998, A&AS, 133, 299
Davidson, K., & Humphreys, R. M. 1997, ARA&A, 35, 1
Duncan, R. A., & White, S. M. 2003, MNRAS, 338, 425
Fernandez Lajus, E., Gamen, R., Schwartz, M., Salerno, N., Llinares, C., Farina, C., Amorin, R., & Niemela, V. 2003, Inf. Bull. Variable Stars, 5477, 1
Grady, C. A., Snow, T. P., Jr., & Timothy, J. G. 1983, ApJ, 271, 691
Iping, R. C., Sonneborn, G., Gull, T. R., Massa, D. L., & Hillier, D. J. 2005, ApJ, 633, L37
Ishibashi, K., Corcoran, M. F., Davidson, K., Swank, J. H., Petre, R., Drake, S. A., Damineli, A., & White, S. 1999, ApJ, 524, 983
Ishibashi, K., et al. 2003, AJ, 125, 3222
Kunasz, P. B. 1980, ApJ, 237, 819
Martin, J. C., Davidson, K., Humphreys, R. M., Hillier, D. J., & Ishibashi, K. 2006, ApJ, 640, 474 (M06)
Morel, T., Georgiev, L. N., Grosdidier, Y., St-Louis, N., Eversberg, T., & Hill, G. M. 1999, A&A, 349, 457
Ninkov, Z., Yang, S., Hill, G. M., & Walker, A. H. 1987, PASP, 99, 284
Pittard, J. M., & Corcoran, M. F. 2002, A&A, 383, 636
Rauw, G., Naze, Y., Carrier, F., Burki, G., Gosset, E., & Vreux, J.-M. 2001, A&A, 368, 212
Rauw, G., et al. 2005, A&A, 432, 985
Repolust, T., Puls, J., & Herrero, A. 2004, A&A, 415, 349
Smith, N. 2002, MNRAS, 337, 1252
Smith, N., Gehrz, R., Hinz, P. M., Hoffmann, W. F., Hora, J. L., Mamajek, E. E., & Meyer, M. R. 2003, AJ, 125, 1458
Smith, N., Morse, J. A., Collins, N. R., & Gull, T. R. 2004, ApJ, 610, L105
Smith, R. K., Brickhouse, N. S., Liedahl, D. A., & Raymond, J. C. 2001, ApJ, 556, L91
Soker, N. 2001, MNRAS, 325, 584
———. 2003, ApJ, 597, 513
———. 2004, ApJ, 612, 1060
———. 2005a, ApJ, 619, 1064
———. 2005b, ApJ, 635, 540
Stahl, O., Weis, K., Bomans, D. J., Davidson, K., Gull, T. R., & Humphreys, R. M. 2005, A&A, 435, 303
Steiner, J. E., & Damineli, A. 2004, ApJ, 612, L133 (SD04)
Stevens, I. R., & Kallman, T. R. 1990, ApJ, 365, 321 (SK90)
Thackeray, A. D. 1953, MNRAS, 113, 211
van Genderen, A. M., de Groot, M. J. H., & The, P. S. 1994, A&A, 283, 89
van Genderen, A. M., Sterken, C., de Groot, A., & Burki, G. 1999, A&A, 343, 847
van Genderen, A. M., et al. 1995, A&A, 304, 415
Venero, R. O. J., Cidale, L. S., & Ringuelet, A. E. 2002, ApJ, 578, 450
Verner, E., Bruhweiler, F., & Gull, T. 2005, ApJ, 624, 973
Whitelock, P. A., Feast, M. W., Marang, F., & Breedt, E. 2004, MNRAS, 352, 447
Zanella, R., Wolf, B., & Stahl, O. 1984, A&A, 137, 79